THE JOURNAL OF BIOLOGICAL CHEMISTRY VOL. 281, NO. 3, pp. 1449–1460, January 20, 2006


# Glutamic Acid-rich Proteins of Rod Photoreceptors Are Natively Unfolded*[S]

Received for publication, May 6, 2005, and in revised form, September 7, 2005 Published, JBC Papers in Press, November 9, 2005, DOI 10.1074/jbc.M505012200

**Renu Batra-Safferling[‡], Karin Abarca-Heidemann[‡§], Heinz Gerd Körschen[‡], Christos Tziatzios[¶], Matthias Stoldt[‖**], Ivan Budyak[‖], Dieter Willbold[‖**], Harald Schwalbe[§], Judith Klein-Seetharaman[§‖], and U. Benjamin Kaupp[‡1]**

*From the [‡]Institut für Biologische Informationsverarbeitung 1 and the [‖]Institut für Biologische Informationsverarbeitung 2, Forschungszentrum Jülich, 52425 Jülich, **Institut für Physikalische Biologie, Heinrich-Heine-Universität, 40225 Düsseldorf, [§]Zentrum für Biologische Magnetische Resonanz/Institut für Organische Chemie und Biochemie, J. W. Goethe-Universität Frankfurt, Marie-Curie-Strasse 11, 60439 Frankfurt, and [¶]Institut für Biophysik, J. W. Goethe-Universität, 60590 Frankfurt, Germany*

**The outer segment of vertebrate photoreceptors is a specialized compartment that hosts all the signaling components required for visual transduction. Specific to rod photoreceptors is an unusual set of three glutamic acid-rich proteins (GARPs) as follows: two soluble forms, GARP1 and GARP2, and the N-terminal cytoplasmic domain (GARP′ part) of the B1 subunit of the cyclic GMP-gated channel. GARPs have been shown to interact with proteins at the rim of the disc membrane. Here we characterized native GARP1 and GARP2 purified from bovine rod photoreceptors. Amino acid sequence analysis of GARPs revealed structural features typical of "natively unfolded" proteins. By using biophysical techniques, including size-exclusion chromatography, dynamic light scattering, NMR spectroscopy, and circular dichroism, we showed that GARPs indeed exhibit a large degree of intrinsic disorder. Analytical ultracentrifugation and chemical cross-linking showed that GARPs exist in a monomer/multimer equilibrium. The results suggested that the function of GARP proteins is linked to their structural disorder. They may provide flexible spacers or linkers tethering the cyclic GMP-gated channel in the plasma membrane to peripherin at the disc rim to produce a stack of rings of these protein complexes along the long axis of the outer segment. GARP proteins could then provide the environment needed for protein interactions in the rim region of discs.**

Photoreceptors transduce the absorption of light into an electrical signal (for review see Ref. 1). The outer segment of vertebrate photoreceptors is a specialized compartment that hosts all the signaling components required for photoelectrical transduction. Rod photoreceptors harbor an unusual set of three glutamic acid-rich proteins (GARP)[2] (see Fig. 1*A*) as follows: two soluble forms, GARP1 and GARP2 (2–4), and a third form, which represents the cytoplasmic N-terminal domain (GARP′ part, almost identical in sequence to GARP1) of the B1 subunit of the cGMP-gated ion channel (5). The B1 subunit and GARP1/GARP2 are derived from a single gene by alternative promoters and splicing (6–8). GARPs are characterized by their extremely high content of glutamate residues (~150 residues in GARP1 and in the GARP′ part) and repetitive sequence motifs, in particular four short repeats designated R1–R4 (2, 3, 5) (Fig. 1*A*). The highest number of glutamate residues is found in a 110-amino acid-long segment toward the C terminus containing 61% glutamate residues, present in GARP1 and GARP′ but not in GARP2. Nonetheless, GARP2 contains approximately twice the number of glutamate residues than typical globular proteins (see supplemental table). GARPs probably serve a function specific to rods, because the GARP′ part is lacking in splice variants of the rod B1 subunit expressed in olfactory sensory neurons (9, 10) and testes (11). Furthermore, the B3 subunit of the cGMP-gated channel of cone photoreceptors, which is encoded by a different gene, has no GARP-related sequences (12), and soluble GARPs are absent in cones.

GARPs have been proposed to organize an oligomeric protein complex near the cGMP-gated channel (3) and to interact with peripherin (13), a protein located at the disc rim (14). The tethering of the GARP′ part to peripherin is expected to produce a circular arrangement of cGMP-gated channels in juxtaposition to the disc rim (13, 15, 16). The distance between the plasma membrane and the disc rim is ~10 nm (17). However, if the GARP′ part adopts a globular shape with a calculated diameter of 6.6 nm, this would be too small to reach for peripherin across the 10-nm gap. Either the GARP′ part adopts an elongated structure or additional proteins, including soluble GARPs, may help to fill that gap.

Here we have studied the structure and hydrodynamic properties of GARP1 and GARP2 by various biophysical techniques. We identify GARPs as members of a class of proteins that, in their native state, are intrinsically unfolded. The unstructured GARP′ part of B1 probably serves as an elongated tether that secures the cGMP-gated channel to the disc rim and thus provides for a unique geometric arrangement of the channel.

## EXPERIMENTAL PROCEDURES

*Calculation of Mean Net Charge (R) and Mean Hydrophobicity (H)*—The mean net charge (*R*) of a protein is determined as the absolute value of the difference between the number of positively and negatively charged residues divided by the total number of amino acid residues. The *R* values of GARP1 and 2 were calculated using the program ProtParam at the EXPASY server (/www.expasy.org/tools). The mean hydrophobicity (*H*) is the sum of normalized hydrophobicities of individual residues divided by the total number of amino acid residues minus 4 residues (to take into account the fringe effects in

* This work was supported by the Schwerpunktprogramm of the Deutsche Forschungsgemeinschaft "Molekulare Sinnesphysiologie" SPP 1025 and the Sofya Kovalevskaya award (Humboldt-Foundation and Zukunftsinvestitionsprogramm der Bundesregierung Deutschland). The costs of publication of this article were defrayed in part by the payment of page charges. This article must therefore be hereby marked "*advertisement*" in accordance with 18 U.S.C. Section 1734 solely to indicate this fact.

[S] The on-line version of this article (available at http://www.jbc.org) contains a table and Figs. 1 and 2.

[1] To whom correspondence should be addressed: Institut für Biologische Informationsverarbeitung 1, FZJ-IBI-1, 52425 Jülich, Germany. Tel.: 492461-614041; Fax: 492461-614216; E-mail: a.eckert@fz-juelich.de.

[2] The abbreviations used are: GARP, glutamic acid-rich protein; $R_S$, Stokes radius; ROS, rod outer segments; DTT, dithiothreitol; bis-Tris, 2-[bis(2-hydroxyethyl)amino]-2-(hydroxymethyl)propane-1,3-diol; PDE, phosphodiesterase; MALDI-TOF, matrix-assisted laser desorption ionization-time-of-flight; NRMSD, normalized root mean square deviation; $BS^3$, bis(sulfosuccinimidyl)suberate; BMDB, 1,4-bismaleimidyl-2,3-dihydroxybutane; PONDR, prediction of natural disordered regions; IUP, intrinsically unstructured protein; rGARP, recombinant GARP; GC, guanylyl cyclase.

the calculation of hydrophobicity). Individual hydrophobicities were determined using the Protscale program at the EXPASY server, selecting the option "Hphob/Kyte and Doolittle," a window size of 5, and a normalized scale from 0 to 1. $H_{\text{Boundary}}$ ($H_b$) was computed as described by Uversky (18): $H_b = (R + 1.15)/2.785$.

*Secondary Structure Predictions*—Secondary structure predictions of repeat peptides (R1–R4) and proteins (GARP1 and GARP2) were carried out using JPRED, PredictProtein, nnPredict, APSSP, and AGADIR available on the EXPASY server.

*PONDR Prediction of GARP Proteins*—Protein sequences were submitted to the PONDR server (www.pondr.com) using the neural network predictor VL-XT (19, 20). Access to PONDR® was provided by Molecular Kinetics (Indianapolis, IN).

*Purification of GARP1 and GARP2*—Rod outer segments (ROS) were prepared from dark-adapted retina as described elsewhere (21). Unless specified, all steps were performed at 4 °C under dim red light. All buffers, except for gel filtration, contained the protease inhibitor mixtures mPIC (Sigma) and Complete (Roche Applied Science) according to the manufacturers' instructions. The rhodopsin content of ROS was determined spectrophotometrically from the absorption at 500 nm using an extinction coefficient of $\epsilon = 40{,}600\ \text{cm}^{-1}\ \text{M}^{-1}$. ROS were suspended in isotonic buffer (20 mM bis-Tris/propane (BTP)), pH 7.4, 120 mM KCl, 0.2 mM $MgCl_2$, 2 mM DTT, to a rhodopsin concentration of 4 mg/ml. The suspension was homogenized and diluted in isotonic buffer to a final rhodopsin content of 1 mg/ml. Additional $MgCl_2$ was added to a final concentration of 2 mM. Membranes were recovered by centrifugation for 20 min at 100,000 × *g* and washed two more times. Under these conditions, GARPs, transducin, and PDE remained in the membrane fraction, whereas most of the other soluble proteins were removed. The membrane pellets were resuspended (1 mg/ml rhodopsin) in hypotonic buffer (5 mM Tris-HCl, pH 7.4, 0.2 mM $MgCl_2$, 5 mM DTT) and illuminated for 5 min. The soluble fraction (containing GARP1, GARP2, and PDE) was separated from the membranes by centrifugation for 20 min at 314,000 × *g*. The pellet was washed twice and stored at 4 °C.

The pooled supernatants of the hypotonic washings were loaded onto a 5-ml TSK heparin column (TosoHaas, Frankfurt, Germany) equilibrated with hypotonic buffer. The column was washed at 1 ml/min with hypotonic buffer until the absorbance reached the base line. GARP1 and -2 bound weakly to the column and eluted when the buffer was changed to TSK-buffer A (25 mM BTP, pH 7.4, 1 mM $MgCl_2$, and 1 mM DTT). After washing with TSK-buffer A, PDE and other proteins were eluted in a gradient of 0–60% TSK-buffer B (TSK-buffer A containing 1 M NaCl). The proteins were collected in 1.5-ml fractions (GARP) or in 3-ml fractions (PDE) and checked by SDS-PAGE with Coomassie Blue staining and Western blotting. GARP1 and -2 eluted from the heparin column were finally separated on a Superdex-200 HiLoad 16/60 column (Amersham Biosciences) with a flow rate of 1 ml/min (20 mM BTP, pH 7.4, 130 mM NaCl, 1 mM $MgCl_2$, 1 mM DTT). GARP1- and GARP2-containing fractions were pooled and concentrated to ~2 mg/ml using Centriplus 30 or Centriplus 10 spin columns (Millipore), respectively. The purity of the samples was analyzed by Coomassie staining. The protein standards used for the calibration of the Superdex columns were as follows: thyroglobulin 669 kDa, ferritin 440 kDa, catalase 232 kDa, aldolase 158 kDa, ovalbumin 44 kDa, and chymotrypsinogen 25 kDa. Blue dextran (2000 kDa) was used to determine the void volume of the column.

*Coomassie Staining of SDS-PAGE*—SDS-polyacrylamide gels were stained overnight by a solution containing 30% (v/v) ethanol, 10% (v/v) acetic acid, and 1% (w/v) Coomassie Brilliant Blue R-250. Destaining was performed by using the same solution without the dye. Under these conditions at least 50 ng of most proteins are visible.

*Construction and Purification of Recombinant GARP2 Expressed in Escherichia coli*—Recombinant GARP2 (rGARP2) was expressed in *E. coli* strain BL21 (DE3) *pLysE* (Novagen) as His-tagged fusion protein using the pET30a vector. Cells were resuspended and sonicated (3 × 10 s) in 10 mM $Na^+$ phosphate, pH 7.0. After addition of DNase (1,000 units/liter culture) and 2 mM $MgCl_2$, the suspension was incubated on ice for 15 min and then centrifuged at 60,000 × *g*. The supernatant, containing recombinant GARP2, was adjusted to binding buffer (20 mM $Na^+$ phosphate, pH 7.0, 35 mM imidazole, 2% glycerol, and 500 mM NaCl) and loaded onto a $CoCl_2$-activated nitrilotriacetic acid-HiTrap column (Amersham Biosciences). The column was washed with 10 volumes of binding buffer and then with 10 volumes of binding buffer containing 100 mM imidazole. Recombinant GARP2 was eluted with binding buffer containing 500 mM imidazole and further purified by size-exclusion chromatography using a Superdex 200 column (Amersham Biosciences).

*Mass Spectrometry*—MALDI-TOF mass spectra of purified native GARP2 samples were obtained by using a MALDI-TOF mass spectrometer (Voyager System 4197, PerSeptive Biosystems Inc., Framingham, MA). The instrument was operated in a linear mode (25-kV acceleration, 93% grid, 0.15% guide wire, and 200-MHz digitizer) and employed delayed extraction (320 ns). The *m/z* scale was calibrated using a mixture of known protein samples as follows: apomyoglobin (16.95 kDa), thioredoxin (11.67 kDa), and their respective dimers. Samples (16–20 μg) were mixed with a saturated solution (10 mg/ml) of sinapinic acid matrix (1:1 v/v) and then mixed with acetonitrile containing 0.1% (w/v) trifluoroacetic acid. The samples were deposited on the probe, air-dried, and inserted into the instrument. Spectra arising from 50 to 100 laser shots were averaged, and a 19-point smoothing of data were utilized for protein samples.

*Dynamic Light Scattering*—Measurements were made with a DynaPro-MS/X (Protein Solutions Inc., Lakewood, NJ) at 20 °C using ~47 μl of 0.5 mg of protein/ml of gel filtration buffer. All samples were either filtered (0.2 μm; Whatman) or centrifuged (5000 × *g*, 5 min) prior to the measurements. Diffusion coefficients were obtained from the analysis of the decay of the scattered intensity autocorrelation function. The hydrodynamic radius could be deduced from the diffusion coefficients using the Stokes-Einstein equation. All calculations were performed using the software Dynamics V6 provided by the manufacturer.

*Quantification of GARPs in ROS*—The amount of GARP proteins relative to each other and to other proteins in the ROS (rhodopsin, PDE) was determined by SDS-PAGE and densitometric image analysis of Western blots on a Kodak Image Station. Three different ROS preparations were used. We performed the Western blot analysis using a polyclonal "anti-GARP" antibody (3) that labels the following three bands: namely the B1 subunit of the cGMP-gated channel, GARP1, and GARP2. The amount of rhodopsin in ROS preparations was determined spectrophotometrically (22). The samples covered a concentration range of 0.1–0.7 μg of rhodopsin. The intensities of bands belonging to each GARP protein in the Western blots were determined densitometrically. The ratio of GARP proteins is a result of two independent experiments performed in duplicate using three different ROS preparations (total of 12 values).

*NMR Spectroscopy*—NMR samples contained 0.125 mM purified rGARP2 protein in 10 mM $Na^+$ phosphate, 120 mM NaCl, pH 5.2 or 6.8, and 95% $H_2O$, 5% $D_2O$. NMR spectra were recorded at 298 K on a Varian Unity INOVA spectrometer operating at a 600-MHz proton frequency equipped with a 5-mm triple resonance probe and *z* axis

pulsed field gradient. Suppression of the water resonance was achieved through the WATERGATE technique (23). For each spectrum a sum of 128 transients was accumulated to achieve a good signal-to-noise ratio. Chemical shifts were referenced against the methyl signal of external sodium 2,2-dimethyl-2-silapentane-5-sulfonate. Data were processed and plotted using the VnmrJ software (Varian Inc., Palo Alto, CA). Natural abundance $^{1}H,^{15}N$-HSQC experiments were measured using standard pulse sequences at 600- and 700-MHz with Bruker spectrometers, each equipped with a 5-mm triple resonance cryoprobe and *z* axis pulsed field gradients. Spectra were acquired at 298 K in 90% $H_2O$, 10% $D_2O$, pH 3. The concentration of the peptides was 1.5 mM in each case. $^{1}H$ chemical shifts were referenced to sodium 3-trimethylsilyl-2,2,3,3,-$d_4$-proprionate at 0.00 ppm, and $^{13}C$ and $^{15}N$ chemical shifts were calculated from the $^{1}H$ frequency (24). HSQC type experiments were obtained and processed using XWINNMR 3.0 (Bruker Inc.) and TOPSPIN 1.3b (Bruker Inc.).

*Circular Dichroism Spectroscopy*—CD spectra were recorded with a Jasco J810 spectropolarimeter. Spectra of purified GARP proteins in CD buffer (5 mM Tris-HCl, pH 7.5, 100 mM $Na_2SO_4$; 5% (v/v) glycerol, 0.25 mM *n*-dodecyl-β-D-maltoside) were recorded as the average of four individual spectral scans in the far-UV region from 190 to 300 nm using a cuvette with a path length of 0.2 cm and the following parameters: instrument sensitivity, 1 millidegrees; response time, 2 s; scan speed, 50 nm/min. Spectra were analyzed using the Dichroweb on-line server (25, 26). Reference data sets 4 and 7 (27, 28) were used, which are compatible with the wavelength range used in this study. To test the reliability of the secondary structure determinations, a number of alternative algorithms were used for the structure calculations as follows: SELCON3 (29, 30), CONTIN (31, 32), and CDSSTR (27, 33, 34). The analysis provided calculated secondary structures and the goodness-of-fit parameter, normalized root mean square deviation (NRMSD). The NRMSD parameter (25) is defined as follows: $\Sigma(\theta_{exp} - \theta_{cal})^2/(\theta_{exp})^2)^{1/2}$ summed over all wavelengths, where $\theta_{exp}$ and $\theta_{cal}$ are the experimental ellipticities and the ellipticities of the back-calculated spectra, respectively. High NRMSD values (>0.1) indicate that the back-calculated and experimental spectra are not in good agreement (25). However, a low NRMSD value is not always sufficient to indicate an accurate analysis. Because Dichroweb defines the NMRSD parameter in the same way for all analyses, the NMRSD parameter provides a direct means to compare the results obtained using different data bases and algorithms and in the selection of the most appropriate reference data set for the relevant protein. The NMRSD values obtained in this study were all well below 0.1.

*Peptide Synthesis*—Peptide sequences corresponding to repeats R1–R4 in GARP sequences were synthesized according to standard protocols (72). R1 (residues 1–14) corresponds to MLGWVQRVLPQPPG; R2 (residues 100–117) corresponds to VLTWLRKGVEKVVPQPAH; R3 (residues 167–184) corresponds to LLRWFEQNLEKMLPQPPK; and R4 (residues 255–271) corresponds to LMAWILHRLEMALPQPV.

*Chemical Cross-linking of Purified GARP2 Protein*—Native GARP2 was purified as described above. The purified protein (100 ng/ml) was adapted to cross-linking conditions (10 mM Hepes/KOH, pH 7.4, 150 mM NaCl, 2 mM $MgCl_2$, 1 mM $CaCl_2$, 1 mM tris(2-carboxyethyl)phosphine hydrochloride), and the cross-linking reaction was carried out by adding 10× stock solution of the amino-specific cross-linker bis(sulfosuccinimidyl)suberate ($BS^3$) or the thiol-specific cross-linker 1,4-bismaleimidyl-2,3-dihydroxybutane (BMDB) at room temperature (35). Final concentrations of the cross-linkers $BS^3$ and BMDB in the reactions were 0.5 mM and 2.5 μM, respectively. Intermediate cross-link products were identified at various times by termination of the reaction with SDS sample buffer. Cross-link products were analyzed by SDS-PAGE and Western blot analysis (35).

*Analytical Ultracentrifugation*—Experiments were performed in a Beckman Optima XL-A ultracentrifuge, using an An-50Ti rotor at a temperature of 4 °C. Absorbance *versus* radius data, $A(r)$ or $A(r,t)$, were recorded at 280 nm. For the sedimentation equilibrium experiments, Epon 6-channel cells with a path length of 1.2 cm were used with sample and reference volumes of 130 and 135 μl, respectively. The experimental $A(r)$ profiles were evaluated as described earlier (36–38), using the computer program DISCREEQ developed by Schuck (39). Sedimentation velocity runs used Epon double sector cells of 1.2 cm optical length. Sample and reference volumes were 380 and 400 μl, respectively. The experimental $A(r,t)$ data were analyzed by the program SEDFIT applying direct boundary modeling with distribution of Lamm equation solutions (40, 41). The partial specific volume, $\bar{\nu}$, of GARP2 and GARP1 in aqueous buffers was calculated from the amino acid composition according to the method of Durchschlag, applying the data set of Cohn and Edsall, as tabulated in Ref. 42. This led to $\bar{\nu} = 0.722$ ml/g for GARP2 and $\bar{\nu} = 0.702$ ml/g for GARP1. The densities and viscosities of the buffers were calculated using the program SEDNTERP (43).

## RESULTS

*Rationale*—GARP proteins display abnormally slow migration in SDS-PAGE (2, 3, 5, 13). The apparent molecular mass ($M_r$) of GARP1 and GARP2 (~130 and ~62 kDa, respectively) is twice as large as that predicted by the amino acid sequence (64.5 and 31.9 kDa, respectively). The electrophoretic mobility of GARP proteins could be anomalously low for a number of different reasons. 1) Bands may represent dimers of GARP1 and GARP2, respectively. 2) The high content of glutamate residues may result in poor binding of SDS and, thereby, reduced mobility. 3) GARPs may adopt an unusual shape. Previous studies have provided evidence that GARP2 associates both with other retinal proteins (3, 13) and with itself (3), raising the possibility that GARPs serve as multivalent scaffolds for macromolecular signaling complexes. Therefore, we performed sequence analysis and studied the structural properties and the oligomeric state of native GARP1 and GARP2 purified from rod photoreceptors.

*Amino Acid Sequence Analysis of GARP1 and GARP2*—We applied a series of predictors of natural disordered regions (PONDR) to GARP1 and GARP2 and their orthologs to identify the regions that are lacking a fixed tertiary structure (19, 20, 44). About 89% of the GARP1 and 80% of the GARP2 sequences are predicted to be disordered (Fig. 1, *D* and *C*, respectively). The high degree of disorder is similar in three other GARP2 orthologs, although they share relatively low sequence identity (55%). Notably, the conserved repeats R1–R4, which are characterized by an invariant Trp residue and a Pro-Gln-Pro triplet separated by mostly conserved residues (Fig. 1*A*, *lower panel*), are the only regions predicted to adopt an ordered conformation. A characteristic of intrinsically unstructured proteins (IUPs) is that they have a distinctive amino acid composition. They are depleted in "order-promoting" residues (Tyr, Cys, Phe, Trp, Ile, and Leu) and enriched in most "disorder-promoting" residues (Pro, Glu, Ser, and Gln) (18, 45). As a consequence, IUPs typically possess a high net charge at neutral pH and low overall hydrophobicity (18, 46). The amino acid composition of GARPs is similar to that of disordered proteins (supplemental table). Indeed, GARPs fall into the class of IUPs because their mean hydrophobicities ($H$) and mean net charge ($R$) obey the equation $H < (R + 1.151)/2.785$ (47). The results for GARPs are shown in Fig. 1*B*. All GARPs are acidic proteins with a low hydrophobicity.

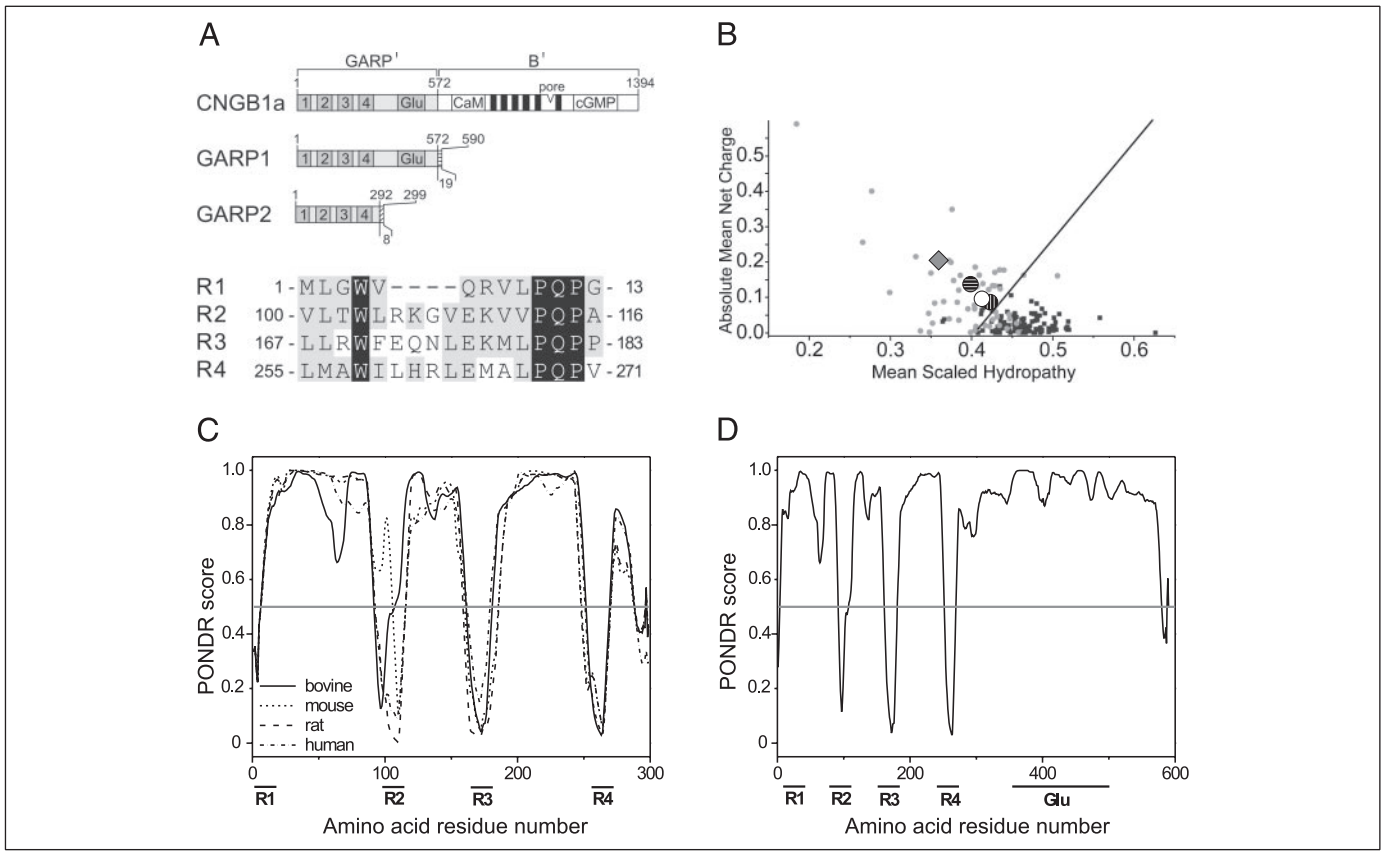


FIGURE 1. **Sequence analysis of GARP proteins.** *A*, *upper panel,* overall organization of GARP sequences, highlighting the four repeats (*1–4*), the glutamic-acid-rich region (*Glu*), a calmodulin-binding site (*CaM*), the transmembrane segments (*black bars*), and the binding site for cGMP. *Lower panel,* amino acid alignment of the four repeats R1–R4 from bovine GARPs. *Black boxes* indicate amino acid identities; *gray boxes* show conservative substitutions. *B*, charge *versus* hydrophobicity plot of GARP proteins. The mean net charge per residue of GARP1 (*diamond*) and GARP2 proteins (*circles*) is plotted *versus* the mean hydrophobicity. Values for a number of known natively unfolded (*small gray circles*) and folded proteins (*black squares*) analyzed previously by Uversky *et al.* (47) are also shown. The line ($H = (R + 1.151)/2.785$), demarcates the boundary between natively unfolded and folded proteins in the charge-hydrophobicity plot. Note that all GARP proteins localize to the natively unfolded region of the charge-hydrophobicity plot. *Gray diamond*, bovine GARP1; *circle* with *vertical lines*, bovine GARP2; *open circle*, human GARP2; *circle* with *horizontal lines*, mouse GARP2. *C*, PONDR of bovine GARP2 and its orthologs; *D*, PONDR of bovine GARP1. Disorder prediction values are plotted against residue number (*thin gray line*). The significance threshold, above which residues are considered to be disordered, is set to 0.5. The results indicate that >75% of the amino acid residues in all GARP proteins fall in the disordered region.

*Purification of Native GARP1 and GARP2*—The purification of native GARPs proceeds in four steps. First, dark-adapted ROS were mechanically disrupted in isotonic buffer. The membranes were washed three times with isotonic buffer. Under these conditions, GARP1, GARP2, the PDE, and transducin stay on the membranes and can be separated from other cytosolic proteins by centrifugation (data not shown). Second, membranes were illuminated and then washed in hypotonic buffer releasing GARPs, PDE, and other proteins from the membranes. Third, GARPs were separated from other proteins, notably PDE, by chromatography using a heparin column (Fig. 2, *A* and *B*). The GARP-containing fractions contained only few additional proteins as revealed by the Coomassie staining procedure that has a detection limit of ~50 ng of protein (Fig. 2*B*). Moreover, Western blotting using antibodies that recognize the $\alpha$ and $\gamma$ subunits of the PDE did not reveal any contamination by PDE of the GARP2-containing fractions eluted from the heparin column (data not shown). Finally, GARP1 and GARP2 were separated from each other by size-exclusion chromatography using a Superdex-200 column (Fig. 2, *C* and *D*). Using this procedure, the proteins were purified to homogeneity as judged from Coomassie-stained gel shown in Fig. 2*D* (*right panel*).

*Abundance of GARPs in Rod Outer Segments*—A constraint that may provide important clues as to the function of GARPs is their relative abundance in rods. Because of the acidic nature of GARPs, Coomassie and Amido Black stains used routinely for protein quantification bind relatively poorly. Therefore, we estimated the relative amount of GARP proteins in ROS by densitometric image analysis of Western blots stained with the antibody anti-GARP (3) directed against the common N-terminal region (Fig. 1*A*, *upper panel*). Because the molar ratios of key proteins in ROS, namely rhodopsin, transducin, PDE, and cGMP-gated channel, are known (1), as well as the subunit stoichiometry of the cGMP-gated channel (one B1 subunit per channel (35, 48, 49)), we could determine the ratios between all three GARP proteins and between GARPs and other components of the signaling cascade. The mean molar ratio of GARP1:B1:GARP2 was 1:5.2 ± 2.5:26 ± 10. The molar ratio of B1:rhodopsin in mammalian rods is 1:1700 (1, 50). The molar ratio of PDE:rhodopsin is roughly 1:310,[3] yielding a GARP2:PDE ratio of approximate unity. Thus, we concluded that GARP2 is a major protein in rod outer segments that is as abundant as PDE.

*Size-exclusion Chromatography*—The elution volume of a protein from a size-exclusion column depends on the hydrodynamic properties of the protein, *i.e.* its mass and shape. For globular proteins, the hydrodynamic radius (or Stokes radius, $R_S$) allows us to deduce an apparent molecular mass. The purification of GARP1 and GARP2 by size-exclusion chromatography revealed that the $R_S$ values for both proteins were significantly larger than would be predicted for a monomer of globular

[3] R. Cote, personal communication.

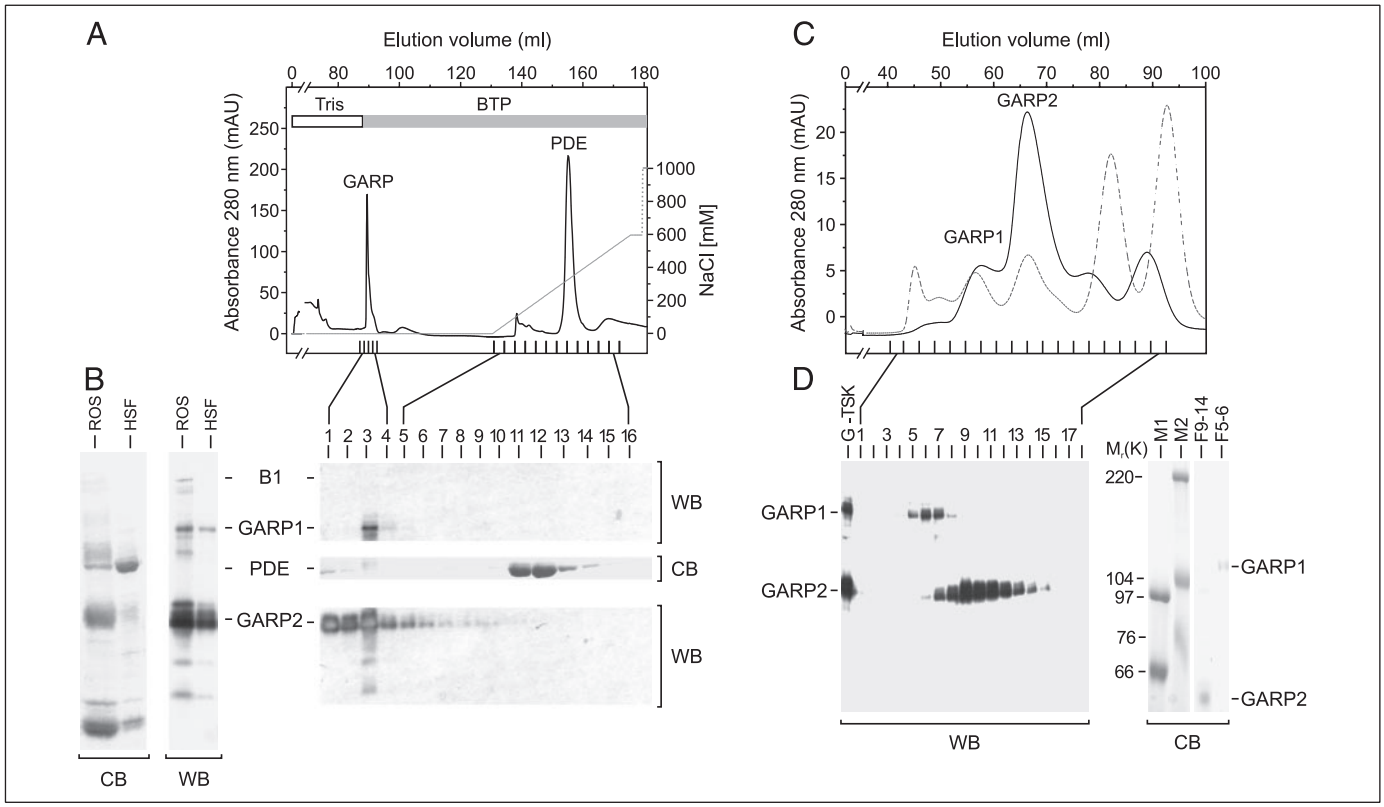


FIGURE 2. **Purification of GARP proteins.** *A*, TSK-heparin column chromatography. The fractions containing GARP1 and GARP2 (*GARP*), which eluted when Tris buffer was exchanged for BTP buffer, as well as the fractions containing PDE eluted with the salt gradient (0–600 mM NaCl), are indicated. *B*, *right panels,* analysis of the GARP-containing fractions and the fractions collected from the NaCl gradient by Western blotting (*B1, GARP1*, and *GARP2*) and by Coomassie staining (*PDE*). *Left panel,* controls, ROS, and the hypotonic soluble fraction (*HSF*) were analyzed by Coomassie staining (*CB*) and by Western blotting (*WB*). Hypotonic soluble fraction was the fraction loaded onto the heparin column. *C*, size-exclusion chromatography. The GARP fractions eluted from the heparin column were pooled (G-TSK) and loaded onto a Superdex-200 column (HR16/60; *black line*). The fractions containing GARP1 and GARP2 are indicated. The peaks of a calibration curve (*dashed line*) correspond to blue dextran (2000 kDa; 44.5 ml), thyroglobulin (669 kDa; 49.3 ml), ferritin (440 kDa; 56.4 ml), catalase (232 kDa; 66 ml), aldolase (158 kDa; 67.7 ml), ovalbumin (44 kDa; 82 ml), and chymotrypsinogen (25 kDa; 92.3 ml). The peaks of catalase and aldolase overlap resulting in a single peak at 66.3 ml. *D*, *left panel,* Western blot analysis (*WB*) of the G-TSK fraction and the fractions eluted from the Superdex-200 column. *Right panel,* Coomassie staining (*CB*) of marker proteins (*M1* and *M2*) and pooled fractions 9–14 (*F9–14*) of GARP2 and pooled fractions 5 and 6 (*F5–6*) of GARP1 eluted from the Superdex-200 column. The Western blot analysis shown in *B* and *D* was performed using the polyclonal antibody FPc52K (anti-GARP) raised against the GARP proteins (3).

shape. Supplemental Fig. 1 shows the elution profile of the purified native GARP2 on a Superdex-200 column. The sharpness of the elution profile indicates that GARP2 migrates as a homogeneous species close to the marker protein catalase (232 kDa). The same profile is obtained irrespective of the buffer composition and the presence of different NaCl concentrations, excluding the possibility of nonspecific interaction of GARP2 with the column matrix (data not shown). Mean $R_S$ values of 65 ± 3 Å ($n$ = 11) (GARP1) and 48 ± 2 Å ($n$ = 11) (GARP2) correspond to ~485 and ~200 kDa, respectively. Thus, the respective molecular mass is up to 8-fold larger than that calculated for monomeric GARP1 (64.5 kDa) and GARP2 (31.9 kDa).

Furthermore, we performed size-exclusion chromatography of purified GARP2 under denaturing conditions in the presence of 6 M guanidinium HCl (supplemental Fig. 1). The elution volume for the denatured GARP2 corresponds to an $R_S$ of 56 Å and ~350 kDa. If compared with a globular protein of the same size, this change in the $R_S$ value upon denaturation is relatively small. Moreover, we estimated the theoretical $R_S$ and hydrodynamic volume ($V_h$) of folded and fully unfolded GARP2 using the equations described by Uversky (18, 51) (Table 1). For GARP2, the theoretical values are 25 Å for $R_S$(fold) and 52 Å for $R_S$(unfold). The theoretical $V_h$ expected for a globular protein composed of 299 amino acid residues is ~71,000 Å$^3$, whereas for a fully denatured protein it would be 508,000 Å$^3$. The experimentally measured $R_S$ value of 48 Å corresponds to a $V_h$ of ~463,000 Å$^3$. We performed similar calculations for GARP1; the values for $R_S$(fold) and $R_S$(unfold) were 33 and 76 Å, respectively, corresponding to $V_h$ values of ~147,000 and ~1,405,000 Å$^3$. The measured $R_S$ value of 65 Å for GARP1 from size-exclusion chromatography corresponds to a $V_h$ value of 1,151,000 Å$^3$. This comparison suggests that GARP proteins either exist as large oligomeric complexes or that the shape of the monomer deviates significantly from that of a globular protein. In fact, the small difference between the $V_h$ of native and guanidinium-denatured GARPs and the small difference between the measured $V_h$ and that calculated for a nonfolded protein suggests that GARPs, in fact, exist in a largely unfolded conformation.

**TABLE 1**

**Stokes radii ($R_s$) and hydrodynamic volumes ($V_h$) for native and fully unfolded GARPs, experimental and theoretical values**

The abbreviations used are as follows: N, native; U, unfolded; MM, molecular mass (in daltons); n, number of amino acid residues.

| Protein | Measured | | Calculated folded | | Calculated unfolded | |
|---|---|---|---|---|---|---|
| | $R_S$ | $V_h$ | $R_S$ (N)[a] | $V_h$ (N)[b] | $R_S$ (U)[c] | $V_h$ (U)[d] |
| | Å | Å$^3$ | Å | Å$^3$ | Å | Å$^3$ |
| GARP1 | 65 | 1,150,679 | 33.2 | 147,012 | 76.1 | 1,405,194 |
| GARP2 | 48 | 463,380 | 25.6 | 70,945 | 52.4 | 507,639 |
| | 56[e] | 735,245 | — | — | — | — |

[a] Log $R_S$ (N) = 0.369 × log (MM) − 0.254.
[b] Log $V_h$ (N) = (2.197 ± 0.037) + (1.072 ± 0.015) × log $n$.
[c] Log $R_S$ (U) = 0.533 × log (MM) − 0.682; $V = 4/3\pi R_S^3$.
[d] Log $V_h$ (U) = (1.997 ± 0.078) + (1.498 ± 0.035) × log $n$.
[e] $R_S$ value of GARP2 measured under denaturing conditions (6 M guanidinium HCl).
[f] —, not applicable.

*Dynamic Light Scattering of Purified Native GARPs*—We examined the hydrodynamic properties of GARPs by another independent technique. Dynamic light scattering is a measure of the diffusion coefficient that depends on the size and shape of the protein. The $R_S$ values for native GARP1 and GARP2 are 76 and 50 Å, respectively. The $R_S$ values varied somewhat for different hydrodynamic techniques (Table 2). Because globular proteins serve as reference for most of the techniques used, we reasoned that the variability in the results obtained for GARP proteins is because of the different influence of conformation on the $R_S$ values obtained by different methods.

*One-dimensional $^1H$ NMR Spectroscopy of Full-length Recombinant GARP2*—NMR chemical shifts carry information on the conformation of proteins. In particular, the existence of the tertiary structure of a protein can be established by one-dimensional proton NMR spectra. Recombinantly expressed and purified GARP2 carrying a His tag was studied by proton NMR spectroscopy. Fig. 3*A* shows proton chemical shifts of rGARP2 at pH 5.2. The spectrum at pH 6.8 was similar to that at pH 5.2 (data not shown). These spectra are similar to those observed for small unstructured peptides (52) and are very different from a folded protein. For comparison, a one-dimensional proton NMR spectrum of carbonic anhydrase, a protein with a molecular mass similar to that of GARP2 and with a stable fold, is shown in Fig. 3*B*. In contrast to carbonic anhydrase, the resonances of the GARP2 protein's methyl group protons (at 0.9 and 0.95 ppm) and amide groups (around 8.4 ppm) along with very limited spectral dispersion of these signals strongly indicate the lack of stable tertiary structure. The presence of isolated or residual secondary structure elements cannot be excluded by proton NMR data alone.

**TABLE 2**

**Hydrodynamic properties of GARP proteins using various biophysical techniques**

| Method of analysis | Calculated/apparent mass and $R_S$[a] | | | |
|---|---|---|---|---|
| | GARP1 | | GARP2 | |
| | Mass | $R_S$ | Mass | $R_S$ |
| | *kDa* | *Å* | *kDa* | *Å* |
| Amino acid composition | 64.5 | 33 | 31.9 | 25 |
| SDS-gel electrophoresis | 130 | —[b] | 62 | — |
| Size-exclusion chromatography | 485 ± 20 | 65 ± 3 (11) | 200 ± 12 | 48 ± 2 (11) |
| MALDI-TOF | ND[c] | ND | 32 ± 0.02 (2) | ND |
| Dynamic light scattering | 390 ± 30 | 76 ± 5 (4) | 170 ± 10 | 50 ± 4 (5) |
| Native gel electrophoresis | ND | ND | 92 ± 12 (3) | — |

[a] Mean ± S.D. (number of measurements); mass was calculated from the mean Stokes radius.
[b] —, not applicable.
[c] ND, not determined.

*CD Studies on Native GARPs*—To characterize the secondary structure of GARP proteins, we used CD spectroscopy. Far-UV CD spectra allow estimation of α-helical, β-sheet, and random coil content of proteins. Typically, the far-UV CD spectra of polypeptides with extensive α-helical structure display two characteristic negative minima near 208 and 222 nm; β-sheet structure yields a negative minimum at 215 nm; and random coil is characterized by a negative minimum around 200 nm and low ellipticity at 222 nm (see Fig. 3*C*, *dotted line*, for bovine serum albumin). The CD spectra of GARP1 and GARP2 show an intense minimum at 201 and 204 nm, respectively, indicating that unordered regions contribute to the spectrum of both proteins (Fig. 3*C*, *dashed* and *solid lines*, respectively). However, the positions of the minima indicate that both proteins are not entirely composed of random coil. Furthermore, the slight negative ellipticity at 222 nm indicates contributions from α-helical regions. This effect is more pronounced in GARP2 than in GARP1 (Fig. 3*C*).

We have calculated the secondary structure content for GARPs from the far-UV CD spectroscopic data (www.cryst.bbk.ac.uk/cdweb) (25, 26). Best fits were obtained using the CDSSTR algorithm (27, 33, 34),

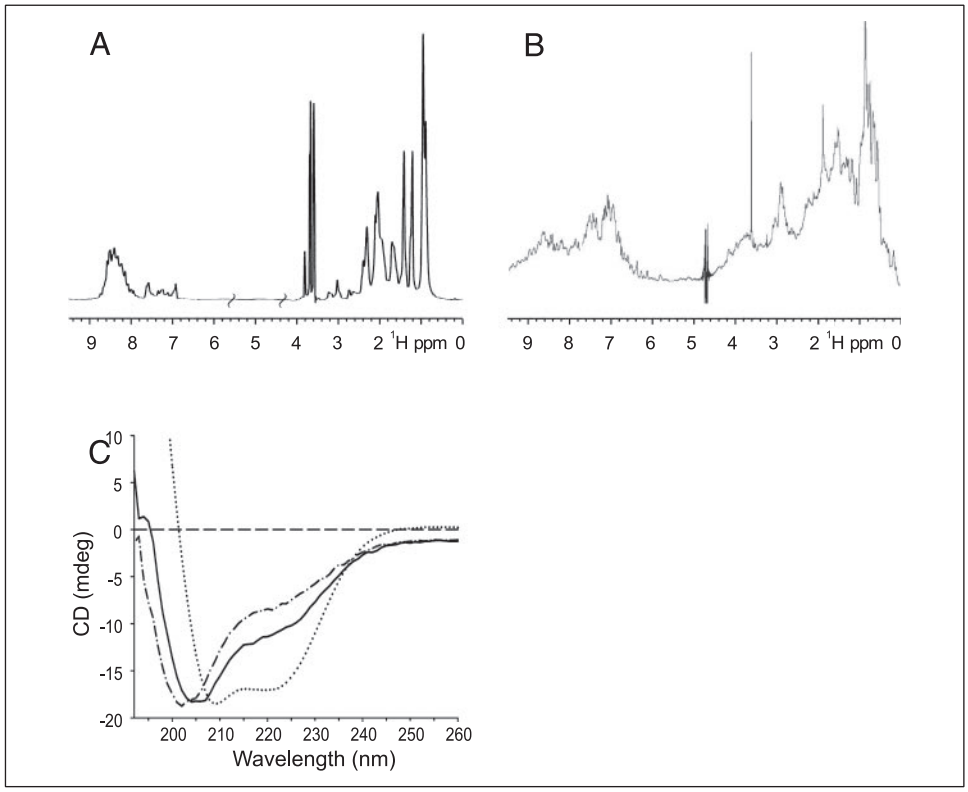


FIGURE 3. **Structural features of GARP proteins.** *A*, analysis of rGARP2 with proton NMR spectroscopy. The one-dimensional proton NMR spectrum of 0.1 mM rGARP2 at pH 5.2 is shown. The spectral region that is affected by suppression of the water signal is indicated. *B*, one-dimensional proton NMR spectrum of carbonic anhydrase (1 and 20 mM sodium phosphate, pH 6, 20% $D_2O$) as a control for a folded protein of size similar to that of GARP2. *C*, analysis of GARP proteins with CD spectroscopy. Far-UV CD spectra of purified native GARP1 (–·–·–), purified native GARP2 (—), and of bovine serum albumin (····) as a control in the same buffer are indicated. All far-UV CD spectra were measured at 25 °C and pH 7.4 in cuvettes with a path length of 0.2 cm; GARP1 is 0.15 mg/ml; GARP2 is 0.1 mg/ml; and bovine serum albumin is 0.15 mg/ml.

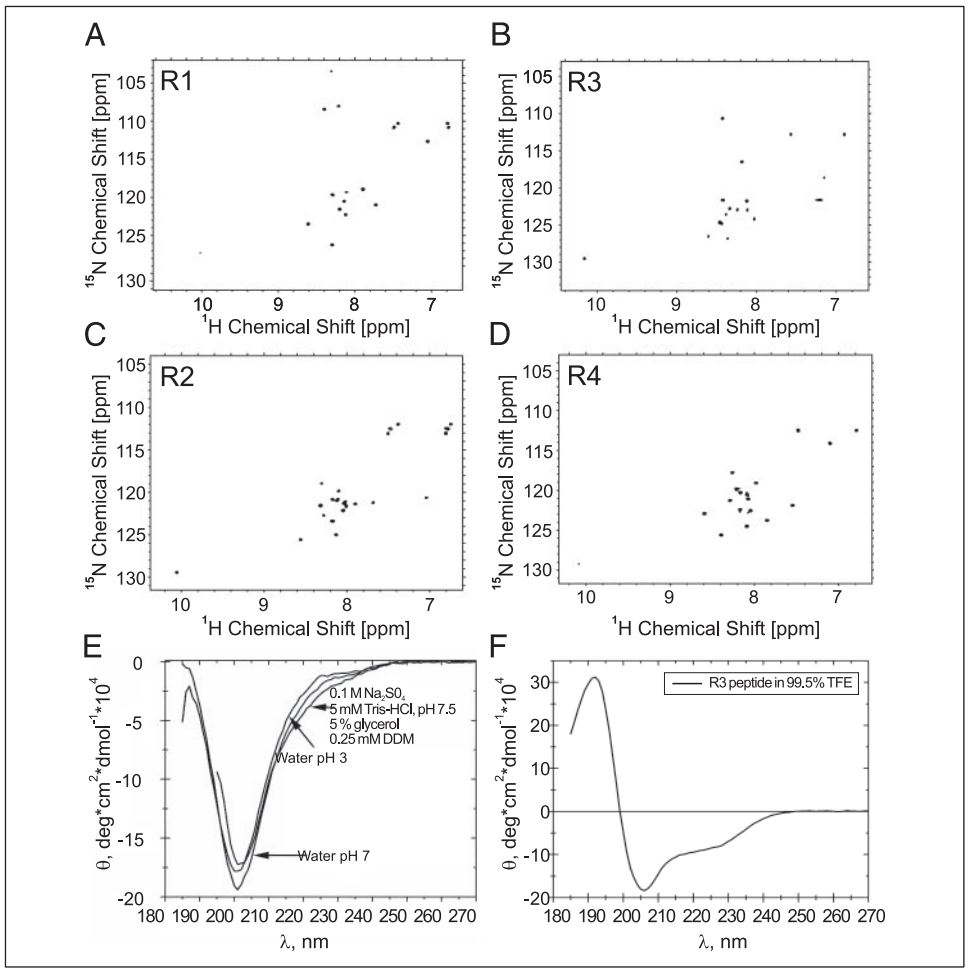


FIGURE 4. **Structural features of peptides containing GARP repeat motifs R1–R4.** *A–D*, natural abundance two-dimensional $^{1}$H,$^{15}$N-HSQC spectra of 1.5 mM unlabeled peptides in 90% $H_2O$, 10% $D_2O$, pH 3, at 298 K. $^{1}$H chemical shifts were referenced to sodium 3-trimethylsilyl-2,2,3,3,-$d_4$-propionate and $^{13}$C and $^{15}$N chemical shifts were calculated from the $^{1}$H frequency (24). The peptides correspond to the following sequences: R1, MLGWVQRVLPQPPG; R2, VLTWLRKGVEKVVPQPAH; R3, LLRWFEQNLEKMLPQPPK; and R4 LMAWILHRLEMALPQPV. *E*, CD spectra of R3 in *water pH 3*, *water pH 7*, and CD buffer used in Fig. 3*B*. Experiments of R1, R2, and R4 gave similar results (data not shown). *F*, CD spectrum of R3 in 99.5% trifluoroethanol (*TFE*). Concentration of peptide was 0.1 mg/ml in all cases.

which predicts an α-helical content of 28% in GARP2 and 11% in GARP1. These results are consistent with the secondary structure prediction obtained from amino acid sequence analysis, which predicts 22 and 13% helical content for GARP2 and GARP1, respectively. Secondary structure is predicted to occur primarily in the regions of the conserved repeats R1–R4. Considering that the length of GARP1 is twice that of GARP2 and assuming that most of the structural content is confined to the repeat regions, we can conclude that the highly charged C-terminal half of GARP1 that is absent in GARP2 is primarily unordered.

*NMR and CD Investigations of Peptides Corresponding to the Repeat Regions*—To test the hypothesis that the repeat regions contribute to the presence of residual structure observed in the overall unfolded GARP proteins, we synthesized four peptides corresponding to the four repeat regions R1–R4 of GARPs, based on the highest propensities for order resulting from the PONDR analysis shown in Fig. 1, *C* and *D*. These peptides (14–18 amino acids long, derived from the sequence of bovine GARPs; Fig. 1*A*, *lower panel*) were subjected to NMR and CD measurements to investigate the presence of tertiary and secondary structure, respectively. Natural abundance $^{15}$N,$^{1}$H-HSQC spectra of R1–R4 peptides in water at pH 3 are shown in Fig. 4, *A–D*. In all four spectra, the resonances are well resolved because of their spectral dispersion. This suggests that these peptides contain tertiary structure elements. The presence of structure in these peptides is also supported by the CD spectra, as shown in Fig. 4*E*. In all four peptides, deconvolution of the spectral components as described above and under "Experimental Procedures" suggests the presence of ~28% β-strand, 15% turn, 3–4% helix, and 54% random coil. The measurements were carried out in water at pH 3 and pH 7, and in the buffer used for the CD measurements of the full-length protein. In the presence of 99% trifluoroethanol (Fig. 4*F*), helix content increased to 23%, decreasing the random coil content to less than 33%, although β-strand and turn contents remained essentially unchanged. Taken together, these results support the notion that peptide repeats R1–R4 are partially structured. Although the full-length protein did not show evidence of β-strand, this is more likely due to the fact that β-structure is more difficult to detect, in particular in the presence of the overwhelming contributions from random coil in the full-length protein. The propensity for helix seen in the full-length protein is encoded in the peptides but requires stabilization through the addition of trifluoroethanol, a known helix inducer (53), and possibly portions of the full-length protein.

*Analytical Ultracentrifugation*—Although the results of size-exclusion chromatography and dynamic light scattering are consistent with the idea that GARPs are largely unstructured, these methods do not exclude the possibility that GARPs form homo-oligomers. This is because of the fact that these techniques cannot distinguish contributions of mass and shape to diffusion. In contrast, analytical ultracentrifugation can be used to determine directly the molar mass or the state of association of macromolecules (54). Therefore, we have carried out analytical ultracentrifugation experiments of GARP1 and GARP2 with and without the nonionic detergent $C_{12}E_9$. The results for GARP2 are shown in Fig. 5, and the results for GARP1 are shown in Fig. 6.

Sedimentation velocity experiments provide a qualitative measure for size and shape distributions of proteins (for review of the method see

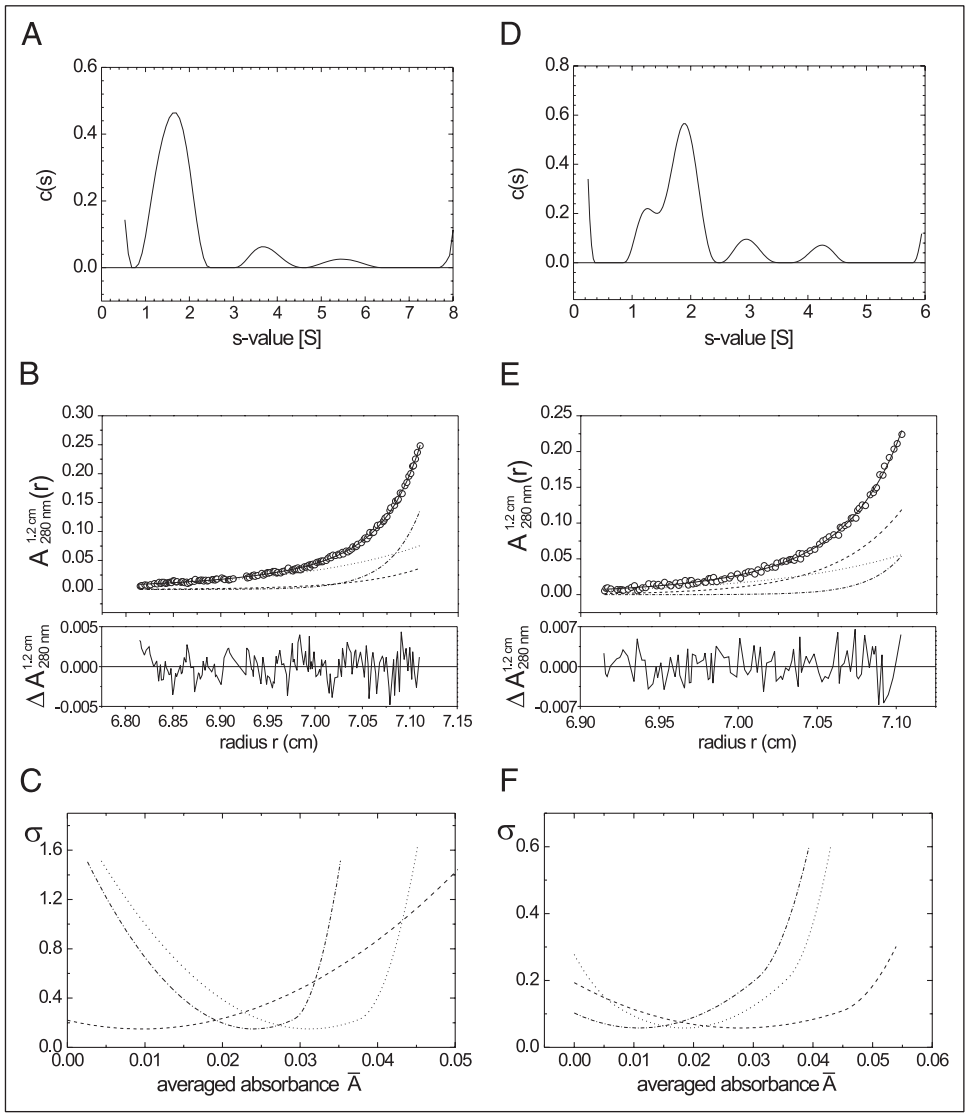


FIGURE 5. **Sedimentation analysis of purified GARP2.** *A–C*, experiments in the absence of detergent. *A*, sedimentation velocity analysis of GARP2. Best fit sedimentation coefficient distribution *c*(*s*), calculated from the experimental sedimentation velocity data *A*(*r*,*t*) by the *c*(*s*) method (40). *B*, sedimentation equilibrium experiment. *Upper panel*, experimental *A*(*r*) data (○), best fit assuming a monomer/dimer/tetramer model of self-association (—), and calculated local contributions of GARP2 monomers (····), dimers (- - - -) and tetramers (–·–·–). *Lower panel*, local differences of Δ*A*(*r*) between experimental and fitted data. *C*, evaluation of the statistical accuracy for the calculated relative absorbance contribution of the different GARP2 oligomers: changes in the sum of the squared residuals, σ, of the fits to the data from *B* that result from one nonoptimal absorbance parameter (37, 39, 57). The minima of the curves correspond to the best-fit values for the relative concentration of each GARP2 oligomer in the sample. Initial protein concentration is $A^{1.2\ cm}_{280\ nm}$ (*r*) = 0.12 (3.75 μM). Solution is 20 mM BTP, pH 7.4, containing 130 mM NaCl, 1 mM $MgCl_2$, and 2 mM DTT. Rotor speed for the sedimentation velocity experiment is 40,000 rpm and for the sedimentation equilibrium experiment is 16,000 rpm. *D–F*, similar experiments as in *A–C* in the presence of the detergent $C_{12}E_9$. The meaning of curves and symbols is the same as that of *A–C*. *D*, sedimentation velocity experiment. *E* and *F*, sedimentation equilibrium experiment. Initial protein concentration is $A^{1.2\ cm}_{280\ nm}$ (*r*) = 0.35 (10.9 μM). Solution is 20 mM BTP, pH 7.4, containing 130 mM NaCl, 1 mM $MgCl_2$, 2 mM DTT and 0.004% (w/v) $C_{12}E_9$. Rotor speed for sedimentation velocity experiment is 45,000 rpm, and for sedimentation equilibrium experiment is 20,000 rpm.

Refs. 55–58). The application of this method to the study of GARP2 in the absence of detergent is shown in Fig. 5*A*. The experimentally observed absorbance as a function of rotor speed and time (*A*(*r*,*t*)) was analyzed using the sedimentation coefficient distribution method, referred to as the *c*(*s*) method (40, 41), which assumes a continuous sedimentation coefficient distribution. A good fit was obtained with a root mean square error of 0.01172 absorbance units. A dominant, broad peak was observed between ~1 S and 2.2 S. Because the relative area under a peak is directly proportional to the concentration of the respective species, we estimated that this peak accounts for ~75% of the total absorbance at 230 nm. The broadness of this signal is indicative of sample heterogeneity. This conclusion is further supported by the presence of several additional minor peaks at higher sedimentation coefficients.

Next, we quantified the underlying cause for heterogeneity observed with sedimentation velocity using the sedimentation equilibrium method under the same experimental conditions. Sedimentation equilibrium studies allow the direct identification of the oligomerization state of a protein in solution (36). The results obtained with GARP2 in the absence of detergent are shown in Fig. 5, *B* and *C*. The *A*(*r*) distributions (Fig. 5*B*) could be fitted with high precision to a model consisting of a mixture of monomers, dimers, and tetramers (Fig. 5*C*). The GARP2 monomer was the predominant component with a relative amount of ~48%, closely followed by the tetramer species (~37%). The smallest component was that of the dimer with ~15% of the total mixture. The addition of higher oligomers ($n > 4$) in the analysis did not improve the quality of the fit. Assuming a mixture of monomers, trimers, and hexamers resulted in a worse fit of the data, increasing the sum of the squared residuals by ~10% (data not shown). Thus, we concluded that GARP2 in the absence of detergent exists as a mixture of monomers, dimers, and tetramers.

In contrast to the results obtained for GARP2, sedimentation equilibrium analysis of GARP1 indicated that the protein was present as an equal mixture of monomers and dimers (Fig. 6*B*). There was no evidence for the presence of higher order oligomers (Fig. 6*A*).

Finally, we examined the possibility that the existence of GARP oligomers results from unspecific aggregation by repeating the above experiments in the presence of $C_{12}E_9$ at concentrations below its critical micellar concentration ($\rho_{C12E9} = 1.05$ g/ml). Fig. 5*D* shows the sedimentation velocity of GARP2 in the presence of 0.004% (w/v) $C_{12}E_9$. The *c*(*s*) analysis of the *A*(*r*,*t*) data resulted in a good fit (root mean square error 0.009133 absorbance units) with a major peak at a position similar to the one observed in the absence of detergent. Again, additional minor peaks were observed at higher sedimentation coefficients. The most signifi-

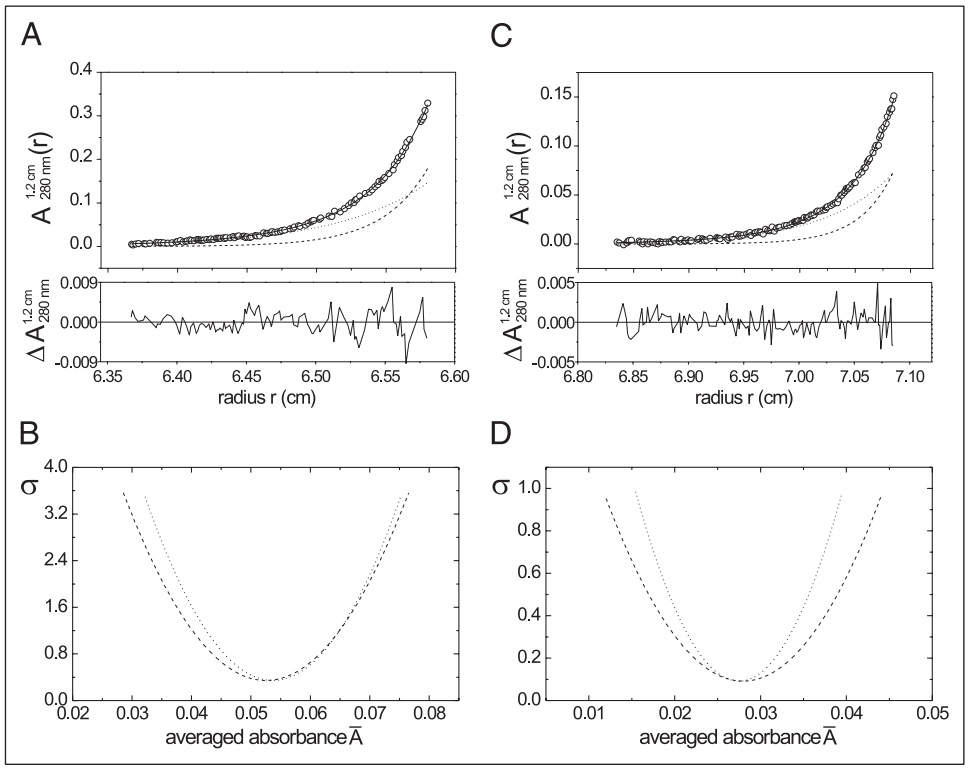


FIGURE 6. **Sedimentation equilibrium analysis of purified GARP1.** *A* and *B*, experiments in the absence of detergent. *A*, sedimentation equilibrium experiment. *Upper panel,* absorbance ($A^{1.2\ cm}_{280\ nm}$) as a function of the radial position *r* (○), and least squares fit to the data assuming the presence of GARP1 monomers and dimers (—). The plot also shows the calculated absorbance contribution of the monomer (····) and dimer (- - - -). *Lower panel,* local differences $\Delta A(r)$ between experimental and fitted data. *B*, statistical analysis as in Fig. 5*C*. Buffer conditions and symbols are as described in Fig. 5, *B* and *C*. *C* and *D*, similar experiments in the presence of the detergent $C_{12}E_9$. The meaning of curves and symbols is the same as that of parts Fig. 5, *B* and *C*. All other conditions are as in Fig. 5, *E* and *F*. Initial protein concentration is $A^{1.2\ cm}_{280\ nm}$ (*r*) = 0.12 (2 μM). Solution is 20 mM BTP, pH 7.4, containing 130 mM NaCl, 1 mM $MgCl_2$, 2 mM DTT and 0.002% (w/v) $C_{12}E_9$. Rotor speed is 16,000 rpm.

cant difference to the results obtained in the absence of detergent was a sharpening of the major peak, which could now be resolved as two separate but overlapping peaks, one with maximum around 1.2 S and the second with maximum around 1.9 S.

Again, the underlying distribution of oligomers was analyzed using sedimentation equilibrium analysis, now in the presence of detergent. The experimental $A(r)$ distributions of GARP2 were fitted perfectly, assuming the presence of monomers, dimers, and tetramers. A typical example is shown in Fig. 5, *E* and *F*. The relative concentrations of the three components in the sample were 33% monomers, 48% dimers, and 19% tetramers. The fit did not improve by considering higher oligomers for the analysis and fits based on a monomer/trimer/hexamer model increased the sum of the squared residuals by more than ~10%. We concluded that the oligomerization state of GARP2 in buffers containing low concentrations of detergent is shifted toward the dimer, significantly reducing the presence of tetramers as compared with in the absence of detergent.

Similar experiments were performed with GARP1 in buffers containing 0.002% (w/v) $C_{12}E_9$ (Fig. 6, *C* and *D*). The experimental $A(r)$ distributions were essentially identical to those observed in the absence of detergent (Fig. 6, *A* and *B*). Excellent fits were obtained by assuming that the protein exists as monomers and dimers, at approximately equal proportions. The consideration of higher oligomers did not improve significantly the quality of the fits. Thus, low concentrations of $C_{12}E_9$ do not affect the association behavior of GARP1, lending credence to the notion that GARP1 dimers are not the result of unspecific aggregation.

*Chemical Cross-linking of Purified GARP2 Protein*—The results of analytical ultracentrifugation establish that under native-like conditions GARPs exist in a monomer-multimer equilibrium. The biophysical characterization of GARP2 shows that it belongs to the class of natively unfolded proteins. This suggests that the low mobility on SDS-PAGE is likely because of the poor binding of SDS and/or the unusual shape rather than dimerization under the SDS-denaturing conditions. Therefore, we concluded that the band of GARP2 (62 kDa) in SDS-PAGE

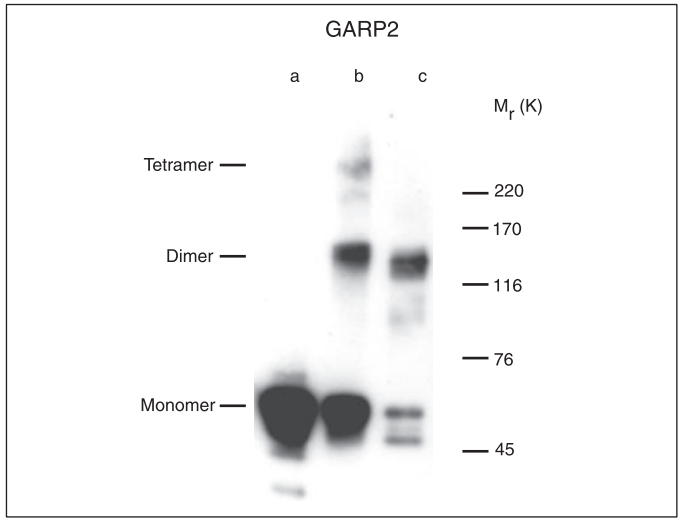


FIGURE 7. **Chemical cross-linking of purified native GARP2 protein.** Purified GARP2 protein (100 ng) was cross-linked with 0.5 mM $BS^3$ (*lane b*) and 2.5 μM BMDB (*lane c*). The reaction was stopped after 1 h, the cross-link products were separated by 4–12% SDS-PAGE and transferred to polyvinylidene difluoride membranes. The Western blot was labeled with polyclonal anti-GARP antibody (3). *Lane a* represents native GARP2 protein before starting the cross-linking reaction.

corresponds to the monomer. To examine further the oligomeric state of GARP2, we studied chemical cross-linking by using two different agents, amino-specific $BS^3$ and thiol-specific BMDB. Incubation of the GARP2 protein with both cross-linking reagents resulted in a decrease of the GARP2 signal corresponding to the monomer on SDS-PAGE, and in the formation of cross-linked products with the molecular mass corresponding to the predicted dimers and tetramers (Fig. 7). The anti-GARP antibody recognized bands of 62, 125, and 246 kDa in case of native GARP2 cross-linked with $BS^3$ (Fig. 7). Native GARP2, when cross-linked using the thiol-specific cross-linker BMDB, resulted in products corresponding to monomers and dimers. In either case,

increasing cross-linking time (up to 3 h) resulted in the total disappearance of the monomeric GARP2 (data not shown). No oligomers higher than tetramers were observed with either cross-linker. These results are consistent with those of the sedimentation equilibrium analysis and strongly support the notion that GARP2 exists as monomers, dimers, and tetramers.

## DISCUSSION

A key finding of this work is that GARPs belong to the class of "natively" unfolded or IUPs. Recent studies have shown that unstructured proteins can be discriminated from globular proteins with high confidence solely on the basis of their sequence (18, 45, 59, 60). The GARP sequences display all the hallmarks of unfolded proteins as follows: low abundance of hydrophobic and order-promoting amino acids and high abundance of charged and disorder-promoting residues resulting in a low hydrophobicity and high net charge. The hydrodynamic properties of GARPs as revealed by dynamic light scattering and size-exclusion chromatography are consistent with an extended conformation. Furthermore, CD and NMR spectra revealed little secondary and tertiary structure. The only regions predicted to be ordered are the conserved repeats R1–R4, each ~14–18 amino acids in length. CD and NMR spectroscopic investigations of peptides corresponding to these repeats experimentally confirmed the presence of significant structure in these regions. The flexible unfolded nature of GARPs was also evident from cryoelectron microscopy studies of the rod cGMP-gated channel, where no electron density could be detected for the GARP′ part in the reconstruction of electron microscopic images (61).

It remains an unanswered question as to what extent IUPs experimentally observed to be unfolded *in vitro* are unfolded *in vivo*. For example, it was shown that FlgM, an intrinsically disordered protein, gains structure inside living *E. coli* cells (62). Because high concentrations of glucose induce the same structure *in vitro*, it is assumed that structure formation *in vivo* is also because of the cellular milieu rather than specific interactions with other proteins. However, it remains a fact that proteins that are observed to be unfolded in dilute solution are thermodynamically less stable than those that maintain their structure in dilute solution. Thus, the low stability of FlgM has been speculated to facilitate secretion through the membrane (62). Generally, it has been suggested that the functions of IUPs fall into five broad categories that are by no means exclusive (45): entropic chains, springs, or bristles, which regulate spacing between components; scavengers, which store or bind small ligands; assemblers, which organize large multiprotein complexes; effectors, which modify the activity of a partner protein; and display sites, which regulate post-translational modifications. GARP proteins may serve several of these functions.

First, because of the interaction with peripherin, the GARP′ part of the B1 subunit tethers the cGMP-gated channel to the disc rim. The tethering is expected to enforce an uneven distribution of the channel in the plasma membrane with a higher concentration at the height of each disc (Fig. 8). The spacing of channel rings along the axis of the outer segment would be determined by the spacing of the discs (300 Å (17)). Because the B1 subunit is much less abundant than peripherin (22, 63, 64), GARP2 may bind to peripherin molecules that are not engaged by the GARP′ part of the B1 channel subunit. Peripherin forms homotetramers and heterotetramers with rom-1 at the rim of discs (64, 65). Considering that GARPs exist in a monomer/dimer/tetramer equilibrium, it is plausible that four GARP molecules interact with tetrameric peripherin. Because cGMP-gated channels contain one B1 subunit and because GARP2 is 5-fold more abundant than B1, it is also plausible that three GARP2 molecules and one B1 subunit interact with peripherin tetramers.

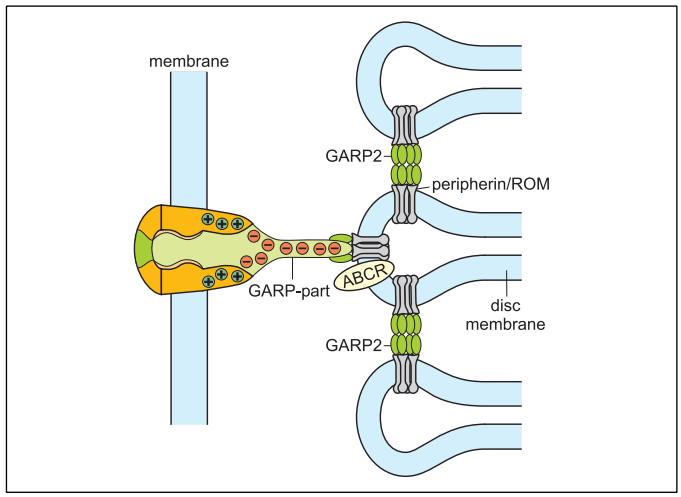


FIGURE 8. **Model of protein-protein interactions between the GARP′ part/GARP2 and the rim of discs.** The GARP′ part and GARP2 are shown in *light* and *dark green*, respectively. For simplicity, the GARP′ part and GARP2 are not drawn to scale. *ABCR*, retinal ATP binding cassette transporter; ROM, integral membrane protein that associates with peripherin-2.

The C terminus of peripherin has been reported to induce membrane fusion (66). The capping of peripherin by GARP2 may prevent fusion of disc and plasma membrane or fusion between discs at the swellings of the disc rim. Moreover, GARP2 molecules could serve as entropic bristles or brushes that control the entry of other proteins into the space between disc and plasma membrane. There is massive light-dependent trafficking of soluble proteins between the outer and inner segment (67). Translocated proteins must travel up and down the outer segment in the small space between disc rim and plasma membrane. It is conceivable that an entropic GARP2 brush is involved in the control of this protein trafficking. Furthermore, GARPs may act as springs in this scenario. A flexible connection might be useful during formation of the disc as it expands and/or during the movement of discs during daily synthesis and turnover for phagocytosis. Electron micrographs reveal filaments between disc and plasma membrane, but also between the rims of adjacent discs (17). It needs to be tested by experiment whether the GARP′ part and GARP2 indeed are involved in forming these filaments. A schematic illustration of this hypothesis is depicted in Fig. 8.

Second, GARPs may also serve as scavengers. The cGMP-gated channel is highly permeable to $Ca^{2+}$ ions (for review see Ref. 15), and about 15% of the dark current through cGMP-gated channels is carried by $Ca^{2+}$ ions (68). The high density of negatively charged glutamate residues in all GARPs, but in particular GARP1 and the GARP′ part of B1, which both contain a region with more than 60% glutamate residues, may serve as a low affinity $Ca^{2+}$ buffer that controls the $Ca^{2+}$ concentration profile inside the cell. Most significantly, the cytosolic N-terminal region of the A1 subunit carries a high density of positively charged amino acids. Not surprisingly, the N terminus is also predicted to be unfolded (supplemental Fig. 2*A*). We propose that the N-terminal ends of the three A1 subunits form a positively charged "fence" that funnels the passage of $Ca^{2+}$ ions from the inner channel mouth to the negatively charged GARP (Fig. 8). In conclusion, the juxtaposition of disc and cGMP-gated channels, the positively charged fence, and the negatively charged GARP′ all may contribute to guide $Ca^{2+}$ fluxes onto the disc surface where the $Ca^{2+}$-dependent signaling molecules rhodopsin kinase and guanylyl cyclase (GC) and their respective modulators recov-

erin and guanylyl cyclase-activating proteins are located (for review see Refs. 69 and 70).

Finally, GARPs may serve as assemblers. The rim region is a specialized compartment that is crowded with proteins. GARPs may organize a multiprotein complex at the disc rim (3). By using peptide affinity chromatography, Körschen *et al.* (3) found that retinal ATP binding cassette (ABCR) transporter, PDE, and GC interact with peptides representing repeats R1–R4, although by using co-immunoprecipitation, no interaction was detected with ABCR and GC (13). Unstructured proteins are inherently flexible, and their local and global structures can be easily shaped by their environment. In fact, unstructured proteins or domains are often induced to fold by interaction with other proteins or ligands. Such plasticity might allow a protein to recognize and interact with multiple biological targets without sacrificing specificity. The price of coupled folding and binding is that free energy must be expended to promote an induced folding transition. Consequently, the interaction is expected to result in binding of lower affinity. Moreover, the affinity with which an unstructured protein binds to its target may be controlled by other proteins within an oligomeric complex. Therefore, the findings by Körschen *et al*. (3) and Poetsch *et al*. (13) may be reconciled by assuming multiple and dynamic interactions ranging from low to high binding affinities. It is noteworthy that only a small fraction of GARP2 interacts with peripherin (<10%) (13), suggesting that the interaction is in fact weak, and a stronger interaction may require the presence of additional partners in a physiological milieu provided by the photoreceptor. Mice that are lacking the B1 gene failed to respond to light, because trafficking of the A1 subunit to the outer segment is abolished, whereas the initial morphology of the rod was intact (71). These findings suggest that the interaction between the B1 subunit and the disc rim is important for targeting of the channel to the outer segment rather than for the integrity of the rod morphology.

Which domains of GARPs and peripherin are involved in the interactions? Repetitive segments have been shown to carry crucial function(s) in some of the well characterized IUPs (45, 60). In fact, peptides representing the four repeats interact with several other proteins of ROS, including the ABC transporter, GC, and PDE (3). Most significantly, from the 63-residue-long C terminus of peripherin, 35 residues are predicted to be intrinsically unfolded (supplemental Fig. 2*B*). It needs to be shown by future work whether R1–R4 are involved in binding peripherin and whether the C-terminal end of peripherin undergoes a folding transition upon binding of GARPs. Because peripherin forms tetramers or higher order oligomers, each of the four repeats may interact with one peripherin subunit only. Furthermore, in the absence of peripherin, the four repeats may assist in forming GARP tetramers.

*Acknowledgments—We thank N. Jordan for technical assistance in cell and protein preparations; Dr. A. Baumann for critical reading of the manuscript; A. Eckert for preparing the manuscript; Dr. J. Butler (MRC, Cambridge, UK) for the initial help with analytical centrifugation runs; Dr. M. Seewald (MPI, Dortmund, Germany) for initial help with dynamic light scattering measurements; Dr. S. Grzesiek (Basel, Switzerland) for initial help with NMR spectroscopy; Dr. M. Bott (Jülich, Germany) for mass spectrometry, and Dr. R. Cote (Durham, NC) for many helpful discussions.*

## REFERENCES


1. Pugh, E. N., Jr., and Lamb, T. D. (2000) in *Handbook of Biological Physics* (Stavenga, D. G., DeGrip, W. J., and Pugh, E. N. Jr., eds) pp. 183–255, Elsevier Science Publishers B.V., Amsterdam
2. Colville, C. A., and Molday, R. S. (1996) *J. Biol. Chem.* **271,** 32968–32974
3. Körschen, H. G., Beyermann, M., Müller, F., Heck, M., Vantler, M., Koch, K.-W., Kellner, R., Wolfrum, U., Bode, C., Hofmann, K. P., and Kaupp, U. B. (1999) *Nature* **400,** 761–766
4. Sugimoto, Y., Yatsunami, K., Tsujimoto, M., Khorana, H. G., and Ichikawa, A. (1991) *Proc. Natl. Acad. Sci. U. S. A.* **88,** 3116–3119
5. Körschen, H. G., Illing, M., Seifert, R., Sesti, F., Williams, A., Gotzes, S., Colville, C., Müller, F., Dosé, A., Godde, M., Molday, L., Kaupp, U. B., and Molday, R. S. (1995) *Neuron* **15,** 627–636
6. Ardell, M. D., Makhija, A. K., Oliveira, L., Miniou, P., Viegas-Péquignot, E., and Pittler, S. J. (1995) *Genomics* **28,** 32–38
7. Ardell, M. D., Aragon, I., Oliveira, L., Porche, G. E., Burke, E., and Pittler, S. J. (1996) *FEBS Lett.* **389,** 213–218
8. Ardell, M. D., Bedsole, D. L., Schoborg, R. V., and Pittler, S. J. (2000) *Gene* (*Amst.*) **245,** 311–318
9. Sautter, A., Zong, X., Hofmann, F., and Biel, M. (1998) *Proc. Natl. Acad. Sci. U. S. A.* **95,** 4696–4701
10. Bönigk, W., Bradley, J., Müller, F., Sesti, F., Boekhoff, I., Ronnett, G. V., Kaupp, U. B., and Frings, S. (1999) *J. Neurosci.* **19,** 5332–5347
11. Wiesner, B., Weiner, J., Middendorff, R., Hagen, V., Kaupp, U. B., and Weyand, I. (1998) *J. Cell Biol.* **142,** 473–484
12. Gerstner, A., Zong, X., Hofmann, F., and Biel, M. (2000) *J. Neurosci.* **20,** 1324–1332
13. Poetsch, A., Molday, L. L., and Molday, R. S. (2001) *J. Biol. Chem.* **276,** 48009–48016
14. Molday, R. S., Hicks, D., and Molday, L. (1987) *Investig. Ophthalmol. Vis. Sci.* **28,** 50–61
15. Kaupp, U. B., and Seifert, R. (2002) *Physiol. Rev.* **82,** 769–824
16. Kaupp, U. B., and Tränkner, D. (2004) in *Transduction Channels in Sensory Cells* (Frings, S., and Bradley, J., eds) pp. 209–235, Wiley-VCH, Weinheim
17. Roof, D. J., and Heuser, J. E. (1982) *J. Cell Biol.* **95,** 487–500
18. Uversky, V. N. (2002) *Protein Sci.* **11,** 739–756
19. Li, X., Romero, P., Rani, M., Dunker, A. K., and Obradovic, Z. (1999) *Genome Inform. Ser. Workshop Genome Inform.* **10,** 30–40
20. Romero, P., Obradovic, Z., Li, X., Garner, E. C., Brown, C. J., and Dunker, A. K. (2001) *Proteins* **42,** 38–48
21. Schnetkamp, P. P. M., and Daemen, F. J. M. (1982) *Methods Enzymol.* **81,** 110–116
22. Moritz, O. L., and Molday, R. S. (1996) *Investig. Ophthalmol. Vis. Sci.* **37,** 352–362
23. Piotto, M., Saudek, V., and Sklenar, V. (1992) *J. Biomol. NMR* **2,** 661–665
24. Wishart, D. S., Bigam, C. G., Yao, J., Abildgaard, F., Dyson, H. J., Oldfield, E., Markley, J. L., and Sykes, B. D. (1995) *J. Biomol. NMR* **6,** 135–140
25. Whitmore, L., and Wallace, B. A. (2004) *Nucleic Acids Res.* **32,** 668–673
26. Lobley, A., Whitmore, L., and Wallace, B. A. (2002) *Bioinformatics* **18,** 211–212
27. Sreerama, N., and Woody, R. W. (2000) *Anal. Biochem.* **287,** 252–260
28. Sreerama, N., Venyaminov, S. Y., and Woody, R. W. (2000) *Anal. Biochem.* **287,** 243–251
29. Sreerama, N., and Woody, R. W. (1993) *Anal. Biochem.* **209,** 32–44
30. Sreerama, N., Venyaminov, S. Y., and Woody, R. W. (1999) *Protein Sci.* **8,** 370–380
31. Provencher, S. W., and Glockner, J. (1981) *Biochemistry* **20,** 33–37
32. Van Stokkum, I. H. M., Spoelder, H. J. W., Bloemendal, M., Van Grondelle, R., and Groen, F. C. A. (1990) *Anal. Biochem.* **191,** 110–118
33. Compton, L. A., and Johnson, W. C., Jr. (1986) *Anal. Biochem.* **155,** 155–167
34. Manavalan, P., and Johnson, W. C., Jr. (1987) *Anal. Biochem.* **167,** 76–85
35. Weitz, D., Ficek, N., Kremmer, E., Bauer, P. J., and Kaupp, U. B. (2002) *Neuron* **36,** 881–889
36. Schubert, D., and Schuck, P. (1991) *Prog. Colloid Polym. Sci.* **86,** 12–22
37. Schuck, P., Legrum, B., Passow, H., and Schubert, D. (1995) *Eur. J. Biochem.* **230,** 806–812
38. Musco, G., Tziatzios, C., Schuck, P., and Pastore, A. (1995) *Biochemistry* **34,** 553–561
39. Schuck, P. (1994) *Prog. Colloid Polym. Sci.* **94,** 1–13
40. Schuck, P. (2000) *Biophys. J.* **78,** 1606–1619
41. Lebowitz, J., Lewis, M. S., and Schuck, P. (2002) *Protein Sci.* **11,** 2067–2079
42. Durchschlag, H. (1986) in *Thermodynamic Data for Biochemistry and Biotechnology* (Hinz, H. J., ed) pp. 45–128, Springer-Verlag, Berlin
43. Laue, T. M., Shah, B. D., Ridgeway, T. M., and Pelletier, S. L. (1992) in *Analytical Ultracentrifugation in Biochemistry and Polymer Science* (Harding, S. E., Rowe, A. J., and Horton, J. C., eds) pp. 90–125, Royal Society of Chemistry, Cambridge, UK
44. Romero, P., Obradovic, Z., Kissinger, C. R., Villafranca, J. E., Garner, E., Guilliot, S., and Dunker, A. K. (1997) *IEEE Int. Conf. Neural Networks* **1,** 90–95
45. Tompa, P. (2002) *Trends Biochem. Sci.* **27,** 527–533
46. Dunker, A. K., Brown, C. J., Lawson, J. D., Iakoucheva, L. M., and Obradovic, Z. (2002) *Biochemistry* **41,** 6573–6582
47. Uversky, V. N., Gillespie, J. R., and Fink, A. L. (2000) *Proteins Struct. Funct. Genet.* **41,** 415–427
48. Zhong, H., Molday, L. L., Molday, R. S., and Yau, K.-W. (2002) *Nature* **420,** 193–198
49. Zheng, J., Trudeau, M. C., and Zagotta, W. N. (2002) *Neuron* **36,** 891–896
50. Molday, R. S., and Kaupp, U. B. (2000) in *Molecular Mechanisms in Visual Transduction* (Stavenga, D. G., DeGrip, W. J., and Pugh, E. N., Jr., eds) pp. 143–181, Elsevier/North-Holland Biomedical Press, Amsterdam
51. Uversky, V. N. (1993) *Biochemistry* **32,** 13288–13298
52. Bundi, A., and Wüthrich, K. (1979) *Biopolymers* **18,** 285–297

53. Jasanoff, A., and Fersht, A. R. (1994) *Biochemistry* **33,** 2129–2135
54. Cantor, C. R., and Schimmel, P. R. (1980) *Biophysical Chemistry, Part II*, pp. 591–641, W. H. Freeman & Co., New York
55. Schubert, D., Tziatzios, C., Schuck, P., and Schubert, U. S. (1999) *Chem. Eur. J.* **5,** 1377–1383
56. Ziegler, C., Morbach, S., Schiller, D., Kraemer, R., Tziatzios, C., Schubert, D., and Kuehlbrandt, W. (2004) *J. Mol. Biol.* **337,** 1137–1147
57. Tziatzios, C., Schubert, D., Lotz, M., Gundogan, D., Betz, H., Schägger, H., Haase, W., Duong, F., and Collinson, I. (2004) *J. Mol. Biol.* **340,** 513–524
58. Tziatzios, C., Schubert, D., Schuck, P., Lancaster, C. R. D., Gennis, R. B., and Barquera, B. (2004) *Prog. Colloid Polym. Sci.* **127,** 48–53
59. Dunker, A. K., Lawson, J. D., Brown, C. J., Williams, R. M., Romero, P., Oh, J. S., Oldfield, C. J., Campen, A. M., Ratliff, C. M., Hipps, K. W., Ausio, J., Nissen, M. S., Reeves, R., Kang, C., Kissinger, C. R., Bailey, R. W., Griswold, M. D., Chiu, W., Garner, E. C., and Obradovic, Z. (2001) *J. Mol. Graphics Modelling* **19,** 26–59
60. Tompa, P. (2003) *BioEssays* **25,** 847–855
61. Higgins, M. K., Weitz, D., Warne, T., Schertler, G. F. X., and Kaupp, U. B. (2002) *EMBO J.* **21,** 2087–2094
62. Dedmon, M. M., Patel, C. N., Young, G. B., and Pielak, G. J. (2002) *Proc. Natl. Acad. Sci. U. S. A.* **99,** 12681–12684
63. Bascom, R. A., Manara, S., Collins, L., Molday, R. S., Kalnins, V. I., and McInnes, R. R. (1992) *Neuron* **8,** 1171–1184
64. Goldberg, A. F., Moritz, O. L., and Molday, R. S. (1995) *Biochemistry* **34,** 14213–14219
65. Loewen, C. J. R., and Molday, R. S. (2000) *J. Biol. Chem.* **275,** 5370–5378
66. Boesze-Battaglia, K., Lamba, O. P., Napoli, A. A., Jr., Sinha, S., and Guo, Y. (1998) *Biochemistry* **37,** 9477–9487
67. Sokolov, M., Lyubarsky, A. L., Strissel, K. J., Savchenko, A. B., Govardovskii, V. I., Pugh, E. N., Jr., and Arshavsky, V. Y. (2002) *Neuron* **33,** 95–106
68. Nakatani, K., and Yau, K.-W. (1988) *J. Physiol.* (*Lond.*) **395,** 695–729
69. Palczewski, K., Polans, A. S., Baehr, W., and Ames, J. B. (2000) *BioEssays* **22,** 337–350
70. Palczewski, K., Sokal, I., and Baehr, W. (2004) *Biochem. Biophys. Res. Commun.* **322,** 1123–1130
71. Huttl, S., Michalakis, S., Seeliger, M., Luo, D. G., Acar, N., Geiger, H., Hudl, K., Mader, R., Haverkamp, S., Moser, M., Pfeifer, A., Gerstner, A., Yau, K.-W., and Biel, M. (2005) *J. Neurosci.* **25,** 130–138
72. Pennington, M. W., and Dunn, B. M. (eds) (1994) *Peptide Synthesis Protocols*, Vol. 35, Humana Press Inc., Totowa, NJ